

Solving efficiently the dynamics of many-body localized systems at strong disorder

Giuseppe De Tomasi,^{1,2} Frank Pollmann,^{1,3} and Markus Heyl²

¹*Technische Universität München, 85747 Garching, Germany*

²*Max-Planck-Institut für Physik Komplexer Systeme, Nöthnitzer Straße 38, 01187-Dresden, Germany*

³*Munich Center for Quantum Science and Technology (MCQST), Schellingstr. 4, D-80799 München, Germany*

We introduce a method to efficiently study the dynamical properties of many-body localized systems in the regime of strong disorder and weak interactions. Our method reproduces qualitatively and quantitatively the time evolution with a polynomial effort in system size and independent of the desired time scales. We use our method to study quantum information propagation, correlation functions, and temporal fluctuations in one- and two-dimensional MBL systems. Moreover, we outline strategies for a further systematic improvement of the accuracy and we point out relations of our method to recent attempts to simulate the time dynamics of quantum many-body systems in classical or artificial neural networks.

Introduction— Experiments in quantum simulators, such as ultra-cold atoms in optical lattices and trapped ions, have nowadays achieved access to the dynamical properties of closed quantum many-body systems far from equilibrium [1–4]. Therefore, it has become possible to experimentally study intrinsically dynamical phenomena that are challenging to realize and probe on other platforms. One prominent example constitutes the many-body localized phase in systems with strong disorder, whose signatures have been observed in a series of recent experiments [5–9]. Many-body localization (MBL) describes a nonergodic phase of matter, in which particles are localized due to the presence of a strong disorder potential [10–13], extending the phenomenon of Anderson localization [14] to the interacting case. Importantly, the presence of interactions makes the dynamical properties much richer [15–21]. In particular, interactions give rise to an additional dephasing mechanism, allowing entanglement and quantum information propagation even though particle and energy transport is absent [15–18, 22]. Describing, however, quantitatively this interaction-induced propagation for large systems beyond exact numerical methods has remained as one of the main challenges.

In this work, we introduce an efficient numerical method to compute the dynamics of weakly-interacting fermions in a fully localized MBL phase. The method is controlled by the interaction strength and we find that the error remains bounded in time over many temporal decades up to the asymptotic long-time dynamics of quantum information transport in MBL systems, which occurs on time scales exponentially in system size. The computational resources for computing local observables and correlation functions in our approach scale only polynomially in system size and are even independent of the targeted time in the dynamics. We utilize the method to study the dynamics of interacting fermions not only in one dimension (1D) but also in two dimensions (2D) for up to 200 lattice sites. After benchmarking our approach by comparing the characteristic entanglement entropy growth with exact diagonalization, we study the

quantum information transport on the basis of the quantum Fisher information [7, 23–28], the logarithmic light-cone in correlation functions [22, 29–36], and temporal fluctuations of observables, both for 1D and 2D. Finally, we point out a connection between our approach and recent ideas to encode quantum states into classical and artificial neural networks.

Models & Methods— At sufficiently strong disorder the MBL eigenstates are expected to be adiabatically connected to the non-interacting ones [37, 38]. In such a case the system is fully described by an extensive number of quasi-local integral of motions $\{\hat{I}_l\}$ [29, 39–46], which emphasize an emerging weak form of integrability [37, 41]. In this case the Hamiltonian of the system exhibits a representation of the following form:

$$\hat{H} = \sum_l J_l^{(1)} \hat{I}_l + \sum_{l,m} J_{l,m}^{(2)} \hat{I}_l \hat{I}_m + \dots, \quad (1)$$

where l enumerates the sites of the underlying lattice. For the considered weakly interacting case, higher-order couplings between the integrals of motion \hat{I}_l become exponentially suppressed in the interaction strength, so that we can terminate the expansion as done in Eq. (1). Moreover, it is expected that $J_{l,m}^{(2)} \sim e^{-d(l,m)/\xi}$ with $d(l,m)$ the spatial distance of the two involved lattice sites l and m and ξ denoting the localization length. While it is expected that this so-called l -bit representation exists, it has remained a central challenge (i) to construct explicitly the integrals of motion $\{\hat{I}_l\}$ and (ii) to make use of the l -bit Hamiltonian to compute its dynamics.

In this work, we show that in the limit of weakly interacting fermions at strong disorder both of these challenges can be efficiently solved. In this limit we can decompose the Hamiltonian $\hat{H} = \hat{H}_0 + \hat{V}$ with \hat{H}_0 a non-interacting Anderson-localized system and \hat{V} the interaction part, whose strength we denote by V . We take as the \hat{I}_l 's the integrals of motion of $\hat{H}_0 = \sum_l \epsilon_l \hat{I}_l$ with $\hat{I}_l = \hat{\eta}_l^\dagger \hat{\eta}_l$ and $\hat{\eta}_l^\dagger$ ($\hat{\eta}_l$) denoting the creation (annihilation) operator for a single-particle Anderson eigenstate ϕ_l with eigenvalue ϵ_l . As a second step, we express

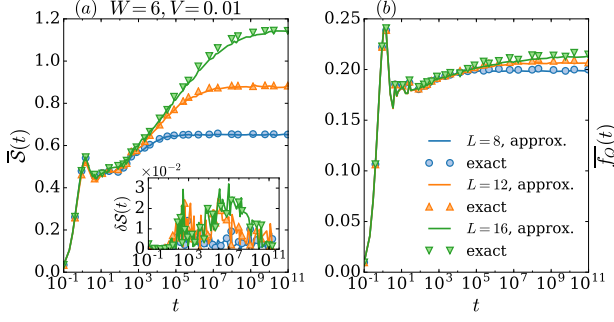


FIG. 1. (a): Bipartite half-chain entanglement entropy $\bar{S}(t)$ after a global quantum quench for several systems sizes (L) in 1D. $\bar{S}(t)$ has been calculated using the exact Hamiltonian \hat{H} (exact) and the effective model \hat{H}^{eff} (approx.). The inset shows the relative error $\delta S(t) = |\bar{S}(t) - \bar{S}^{\text{approx}}(t)| / \bar{S}(t)$, between the entanglement entropy calculated with \hat{H} the one calculated with \hat{H}^{eff} . (b): QFI for the 1D MBL system for several system sizes compared with exact results.

$\hat{V} = \sum_{lmnk} \mathcal{B}_{lmnk} \hat{\eta}_l^\dagger \hat{\eta}_m \hat{\eta}_n^\dagger \hat{\eta}_k$ in terms of the $\{\hat{\eta}_l\}$. Then we neglect all contributions that do not commute with the $\{\hat{I}_l\}$ so that we arrive at the following desired l -bit Hamiltonian:

$$\hat{H}^{\text{eff}} = \sum_l \epsilon_l \hat{\eta}_l^\dagger \hat{\eta}_l + \sum_{l,m} \mathcal{B}_{l,m} \hat{\eta}_l^\dagger \hat{\eta}_l \hat{\eta}_m^\dagger \hat{\eta}_m, \quad (2)$$

with $\mathcal{B}_{l,m} = \mathcal{B}_{llmm} - \mathcal{B}_{lmlm}$. This construction relies on the perturbative nature of an MBL phase, in which the integrals of motion of the system $\{\hat{I}_l\}$ can be obtained perturbatively from the non-interacting ones $\{\hat{\eta}_l^\dagger \hat{\eta}_l\}$ [10, 29, 40, 44, 46]. Thus, as a first approximation in the limit of weak-interactions, the integrals of motion can be taken as the ones of the non-interacting case. In the concluding discussion we will outline how one can improve systematically the accuracy of the l -bits by accounting for higher orders V [47]. For the following, we will use the representation above and show that it is already sufficient to capture quantitatively the dynamics for small V .

Having discussed the construction of the l -bit Hamiltonian, we now outline how this can be used to study dynamics, which is based on two main properties. First, the time evolution of $\hat{\eta}_l$ and $\hat{\eta}_l^\dagger$ can be determined analytically via $\hat{\eta}_l^\dagger(t) = \exp[i t \epsilon_l + i t \sum_m \tilde{\mathcal{B}}_{l,m} \hat{\eta}_m^\dagger \hat{\eta}_m] \hat{\eta}_l^\dagger$ where $\tilde{\mathcal{B}}_{l,m} = \mathcal{B}_{m,l} + \mathcal{B}_{l,m}$. Second, for an initial state $|\psi\rangle$, which is a product states in terms of the bare fermions, i.e. Gaussian, the expectation values of time-evolved local observables and correlation functions can be reduced to the evaluation of Slater determinants, which can be done very efficiently. For example, for a generic local observable $\hat{A} = \sum_{l,m} a_{l,m} \hat{\eta}_l^\dagger \hat{\eta}_m$, we need only to calculate $\langle \hat{\eta}_l^\dagger \hat{\eta}_m(t) \rangle = e^{i t (\epsilon_l - \epsilon_m)} \langle \hat{\eta}_l^\dagger e^{i t \sum_p (\tilde{\mathcal{B}}_{l,p} - \tilde{\mathcal{B}}_{p,m}) \hat{\eta}_p^\dagger \hat{\eta}_p} \hat{\eta}_m \rangle$, where $\langle \dots \rangle =$

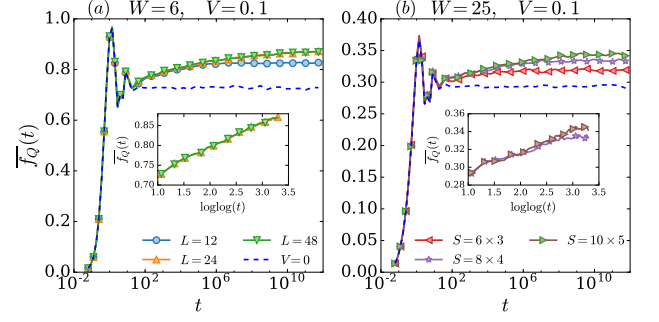


FIG. 2. (a): Disorder averaged QFI-density ($\bar{f}_Q(t) = \bar{\mathcal{F}}_Q(t)/2N$) for the 1D MBL model for several system sizes (L) and a fixed disorder and interaction strength. The inset shows $\bar{f}_Q(t)$ in a suitable scale to underline that $\bar{f}_Q(t) \sim \log \log t$. (b): Disorder averaged QFI-density ($\bar{f}_Q(t)$) for the 2D model for several system sizes (S) and a fixed disorder and interaction strength. The inset shows that also in this case $\bar{f}_Q(t) \sim \log \log t$. For both panels the evolution has been obtained using \hat{H}^{eff} . Dashed-lines are for the non-interacting case ($V=0$) for the largest system size in each panels.

$\langle \psi | \dots | \psi \rangle$. The term $\langle \hat{\eta}_l^\dagger e^{i t \sum_p (\tilde{\mathcal{B}}_{l,p} - \tilde{\mathcal{B}}_{p,m}) \hat{\eta}_p^\dagger \hat{\eta}_p} \hat{\eta}_m \rangle$ can be efficiently computed using Wick's theorem [48], interpreting $e^{i t \sum_p (\tilde{\mathcal{B}}_{l,p} - \tilde{\mathcal{B}}_{p,m}) \hat{\eta}_p^\dagger \hat{\eta}_p}$ as an effective time-evolution operator of the quadratic Hamiltonian $\hat{H}^{(l,m)} = \sum_p (\tilde{\mathcal{B}}_{l,p} - \tilde{\mathcal{B}}_{p,m}) \hat{\eta}_p^\dagger \hat{\eta}_p$. Importantly, such initial conditions are typical choices in theory [15, 20, 21, 49–53] and have been realized in the MBL context experimentally [5, 6, 8, 9].

For concreteness, we demonstrate our method for the Hamiltonian [16, 54–57]

$$\hat{H} := -\frac{1}{2} \sum_{\langle i,j \rangle} (\hat{c}_i^\dagger \hat{c}_j + h.c.) + \sum_j h_j \hat{n}_j + V \sum_{\langle i,j \rangle} \hat{n}_i \hat{n}_j \quad (3)$$

where \hat{c}_j^\dagger (\hat{c}_j) is the fermionic creation (annihilation) operator at site j and $\hat{n}_j = \hat{c}_j^\dagger \hat{c}_j$. $\{h_j\}$ are random fields uniformly distributed between $[-W, W]$, and V is the interaction strength. We study the system both in a 1D lattice of size L with periodic boundary conditions and defined in a rectangular lattice (2D) of size $S = L \times \frac{L}{2}$ with periodic and open boundary conditions respectively in the x and in the y direction. We focus on half-filling $N/L = 1/2$ ($N/|S| = 1/2$) with N the number of fermions. The 1D system is believed to have an MBL-phase at strong-disorder [55–60]. The 2D case on the other hand has largely remained elusive due to the lack of efficient methods to simulate sufficiently large system sizes. A recent experiment has given evidence of an MBL phase in a bosonic 2D system [6]. Nevertheless, it is currently under debate whether MBL can be stable at all in 2D [6, 8, 61–65]. The proposed mechanism for the breakdown of MBL relies on rare resonances which, however, only manifest on very long time scales, below which our

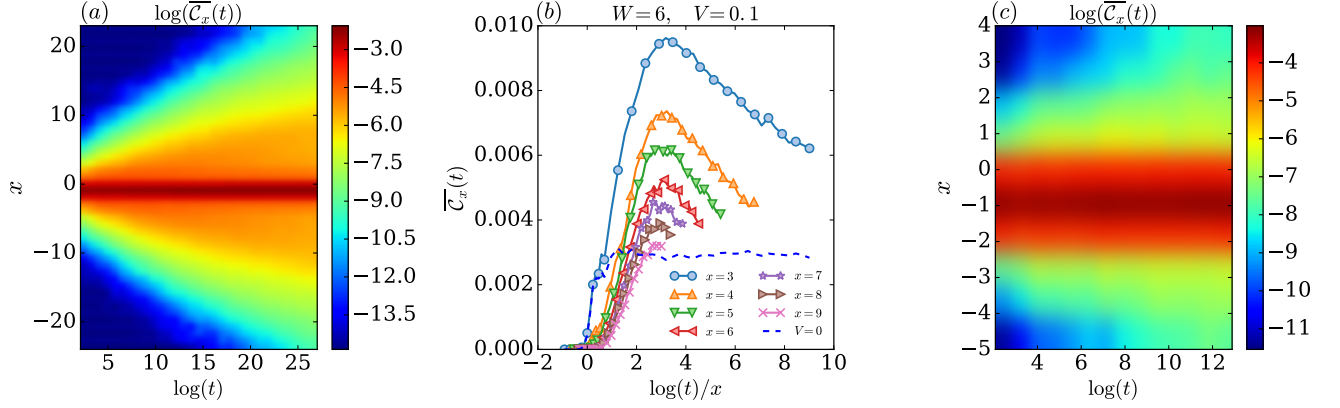


FIG. 3. (a): Logarithmic light-cone calculated using the $\mathcal{C}_x(t)$ for the effective model in 1D. (b): $\mathcal{C}_x(t)$ as a function of time, the time has been properly rescaled to get the collapse of the curves. It also shows the non-interacting case ($V = 0$) (dashed-line). For both panels (a) and (b) $L = 48$. (c): Logarithmic light-cone for the 2D case with $S = 10 \times 5$ in the x -direction calculated using $\mathcal{C}_{x,0}(t)$ evolved with the effective model with $W = 25$ and $V = 0.1$.

l -bit description Eq. 8 could still be accurate at intermediate time scales.

Following our prescription outlined before, we first diagonalize the noninteracting model by introducing $\hat{\eta}_l^\dagger = \sum_i \phi_l(\mathbf{i}) \hat{c}_i^\dagger$. This then leads to $\mathcal{B}_{l,m} = V \sum_{\langle \mathbf{i}, \mathbf{j} \rangle} [|\phi_l(\mathbf{i})|^2 |\phi_m(\mathbf{j})|^2 - \phi_l(\mathbf{i}) \phi_m(\mathbf{i}) \phi_l(\mathbf{j}) \phi_m(\mathbf{j})]$. In the remainder, we choose staggered initial states of charge-density type both for 1D $|\psi\rangle = \prod_{s=-L/4}^{L/4-2} \hat{c}_{2s}^\dagger |0\rangle$ and for 2D $|\psi\rangle = \prod_{y=-L/2}^{L/2-1} \prod_{x=-L/4}^{L/4-2} \hat{c}_{(2x,y)}^\dagger |0\rangle$, motivated by recent experiments [6]. Disorder averaged quantities will be indicated with an overline, e.g. $\langle \hat{n}_i \rangle$.

Benchmark for quantum-information propagation— We now compare the exact dynamics of \hat{H} with the one generated by \hat{H}^{eff} . For the benchmark we choose to study quantum information (entanglement) propagation which inherits one of the central and nontrivial features of MBL phases. In Fig. 1 we show data for two measures both obtained using exact diagonalization and via our effective Hamiltonian [66]. First, this includes the half-chain entanglement entropy

$$\mathcal{S}(t) = -\text{Tr} \hat{\rho}_{L/2}(t) \log \hat{\rho}_{L/2}(t), \quad (4)$$

where $\hat{\rho}_{L/2}(t)$ denotes the reduced density matrix of half of the system. Second, we study the quantum Fisher information (QFI) related to the initial charge-density pattern defined by

$$\mathcal{F}_Q(t) = 4 \left[\langle \hat{\mathcal{O}}(t)^2 \rangle - \langle \hat{\mathcal{O}}(t) \rangle^2 \right], \quad \hat{\mathcal{O}} = \sum_x (-1)^x \hat{n}_x. \quad (5)$$

The QFI probes the propagation of quantum correlations and is an entanglement witness [7, 23–28], that has been also measured experimentally in the MBL context [7].

As we can see from Fig. 1(a) the effective model reproduces not only qualitatively the unbounded logarithmic

growth of the entanglement entropy [15, 42], but even more importantly also quantitatively correctly in the long-time limit. In particular, the inset in Fig. 1(a) shows that the relative error $\delta\mathcal{S}(t) = |\mathcal{S}(t) - \mathcal{S}^{\text{approx}}(t)|/\mathcal{S}(t)$ is a bounded function of time and remains smaller than 3% for all times. Let us note that the results for $\delta\mathcal{S}(t)$ gives evidence that our method not only reproduces the logarithmic growth after disorder averaging but even for individual random configurations. Similarly, also for the QFI the dynamics generated by the effective Hamiltonian follows closely the exact one, see Fig. 1(b) where we define the QFI-density $f_Q = \mathcal{F}_Q/2N$ [7]. While the entanglement entropy serves as a prime example for MBL properties, its computation within our method is not scalable to large system sizes. This, however, is different for the QFI which can still be computed efficiently even for large systems, which allows us to also access it in 2D, see below. It is important to note, that our method reproduces the exact dynamics also for times longer than the naively expected range of validity of perturbation theory ($\sim 1/V$), what can be understood from a statistical analysis of the discarded elements $\mathcal{B}_{l,m,n,k}$ [67].

Results— Having shown that our method reproduces quantitatively the exact dynamics at a controlled error, we now aim to further demonstrate the capabilities of our method. We target this goal by addressing several aspects of MBL systems which up to now have not been accessible or could not be settled due to system size limitations. This includes aspects of quantum information propagation, logarithmic spread of correlations, and temporal fluctuations of local observables both in 1D and 2D. In the following, we choose a larger interaction strength $V = 0.1$ instead of $V = 0.01$ as used for Fig. 1, which increases slightly the relative error in the computed quantities, but on the same time allows us to amplify the

influence of interaction effects.

Figure 2 shows $f_Q(t)$ for the 1D (a) and the 2D case (b), respectively, now computed for much larger systems than done for the benchmark in Fig. 1. For the 2D model we choose the QFI along the x-direction, i.e., $\hat{O} = \sum_x (-1)^x \hat{n}_x$ with $\hat{n}_x := \hat{n}_{(x,0)}$. For comparison we also include the results for the noninteracting models, which show quick saturation to a system-size independent value. For nonvanishing interactions, the behavior of $\overline{\mathcal{F}_Q}(t)$ changes completely and we observe a slow growth, which is consistent with $\overline{\mathcal{F}_Q}(t) \sim \log \log t$ (insets) over many decades in time and almost independent of system size. As a consequence, we are capable to demonstrate slow quantum information propagation in 2D MBL systems, which up to now has not been possible by other methods [29, 61, 64, 65]. In a recent experiment in trapped ions implementing a long-range disordered Ising model evidence for an intermediate $\overline{\mathcal{F}_Q}(t) \sim \log t$ growth has been found [7], which, however, might be due to the fact that the system could be in an algebraic MBL phase [68, 69], leading to $\mathcal{B}_{0,l} \sim 1/l^\beta$ with power-law instead of exponential dependence [68–71].

As a next step we aim at studying quantum correlation spreading via the two-point connected correlation function, defined by

$$C_x(t) = |\langle \hat{n}_x(t) \hat{n}_0(t) \rangle - \langle \hat{n}_x(t) \rangle \langle \hat{n}_0(t) \rangle|. \quad (6)$$

$C_x(t)$ has been used in several quantum systems [31–36] to quantify the time t required to correlate two sites at some distance x , giving rise to the so called light-cone of propagation of correlations. Moreover, $C_x(t)$ has been measured in a recent experiment in a disordered Bose-Hubbard chain to probe the existence of an MBL-phase [30]. The 1D case we address in Fig. 3(a), where we show a color plot of $C_x(t)$ displaying the logarithmic light-cone [30–36, 72, 73] over many decades with quantum correlations spreading in space only logarithmically slowly in time. Interestingly, however, we find that there exists a time scale t_x^* beyond which $C_x(t)$ starts to decrease again, see Fig. 3(b), an effect which has not yet been recognized before. Remarkably, this indicates that quantum correlations are eventually scrambled in the long-time limit also in an MBL system, which might be consistent and even necessary with the expectation to reach in the long-time limit a state with volume-law entanglement entropy [74]. From the rescaling of the time axis used in Fig. 3(b) we find evidence that this correlation time t_x^* scales exponentially with the distance x ($\log t_x^* \sim x$). In the case of an Anderson insulator ($V = 0$) quantum correlations are frozen in the long-time limit [15, 42], implying the saturation to non-zero value of $C_x(t)$ (Fig. (b) 3 dashed-line). Finally, in Fig. (c) 3 we study correlation spreading in 2D, where we found again, like in 1D, the same logarithmically slow propagation.

As opposed to an Anderson insulator it has been argued that an MBL system can show relaxation [60, 75],

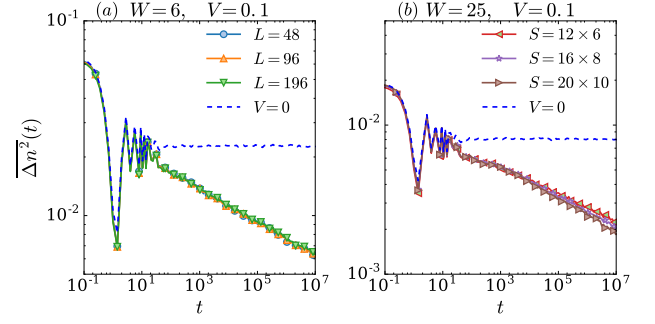


FIG. 4. (a): Disorder average time fluctuations ($\overline{\Delta n^2}(t)$) for several system sizes L for the 1D case, $\overline{\Delta n^2}(t) \sim t^{-\alpha}$. (b): $\overline{\Delta n^2}(t)$ for several system sizes S for the 2D case, also in this case its decay is consistent with an algebraic decay in time. The non-interacting case ($V = 0$) is also shown (dashed-lines) for the largest system size. For both cases the evolution has been performed using \hat{H}^{eff} .

meaning that expectation values of local observables reach at long time a stationary value in the thermodynamic limit with decaying temporal fluctuations. Here, we use our method to reexamine the temporal fluctuations in 1D and to study them also for 2D systems. These are defined for \hat{n}_x via

$$\Delta n^2(t) = \frac{1}{L} \sum_x \Delta n_x^2(t), \quad \Delta n_x^2(t) = (\langle \hat{n}_x \rangle(t) - \langle \hat{n}_x \rangle_{\text{tav}})^2, \quad (7)$$

where $\langle \hat{n}_x \rangle_{\text{tav}}$ denotes the long-time average of $\langle \hat{n}_x \rangle(t)$. As shown in Fig. 4, both in 1D and 2D the temporal fluctuations exhibit an algebraic decay with time, $\overline{\Delta n^2}(t) \sim t^{-\alpha}$. As a reference we have included also the data for the noninteracting cases ($V = 0$, dashed-lines), where temporal fluctuations remain non vanishing for all times. We find that the exponent α is proportional to the single-particle localization length ξ_{loc} [76], for which we now aim to give an analytical argument. This shows that our method not only can be used for numerically computing quantities but also for analytical predictions. For that purpose we consider a special initial state $|\psi\rangle = \prod_l^L \frac{\hat{n}_l + \hat{n}_l^\dagger}{\sqrt{2}} |0\rangle$ for which the calculations are simplified but which gives qualitatively the same decay of the temporal fluctuations [77]. For this state we find $\Delta n_x^2(t) = [\sum_{l \neq m} \phi_l(x) \phi_m(x) e^{i(\epsilon_l - \epsilon_m)t} Q_{lm}]^2$ with $Q_{lm} = 2^{-2} \prod_{k=l+1}^m \sin(A_k^{l,m} t) \prod_{s \neq k} \cos(A_s^{l,m} t)$ and $A_k^{l,m} = (V/2)(\tilde{\mathcal{B}}_{m,k} - \tilde{\mathcal{B}}_{l,k}) \sim V e^{-\frac{\min(|m-k|, |l-k|)}{\xi_{\text{loc}}}}$. The sum over (l, m) can be restricted only to eigenstates, whose centers are located within a distance ξ_{loc} away from x . Each term of the cos's and sin's with argument $A_k^{l,m}$ decays exponentially in k , which leads to a power-law in time [51] with an exponent proportional to ξ_{loc} , implying $\Delta n_x^2(t) \sim t^{-c\xi_{\text{loc}}}$ [20].

Conclusions— In this work, we have formulated a

method which allows to efficiently study the dynamics of weakly-interacting localized fermions. The accuracy of the approach can be further increased systematically by taking into account those contributions to the interaction term, which are not commuting with the bare integrals of motion \hat{I}_l and which have been completely neglected in the present study. For example, to lowest order they can be accounted for by a Schrieffer-Wolff transformation. Our method can be applied to any weakly interacting MBL system, which exhibits an l -bit representation, not only limited to the quantum quench dynamics studied here. Thus, it can be used also to study, for example, also driven Floquet MBL systems [78] such as they appear in discrete time crystals [79, 80], MBL bosonic systems, algebraic MBL [68–70] and MBL weakly coupled with thermal baths [81–84]. However, let us note that even in cases where an MBL phase might not be stable asymptotically for infinite system sizes and infinite times, our method might still provide a description on intermediate time scales (e.g. MBL in 2D [6, 8, 61–65]).

Overall, our method maps the dynamical quantum many-body problem onto a system of classical degrees of freedom of mutually commuting operators, similar in spirit to recent works where dynamical problems have been solved using classical [85] or artificial neural networks [86]. Instead of solving the problem in the basis of the bare particles, our work shows that a simple basis transformation onto more convenient degrees of freedom can improve the accuracy and efficiency dramatically, which might also be of relevance for the aforementioned approaches.

Note—Very recently the dynamics of one-point functions has been computed using a self-consistent Hartree-Fock method, which scales polynomially in system-size and time [87].

Acknowledgments— We thank J.H. Bardarson, S. Bera, A. Burin, A. Eckardt, I. M. Khaymovich, M. Knap and D. Trapin for several illuminating discussions. FP acknowledges the support of the DFG Research Unit FOR 1807 through grants no. PO 1370/2- 1, TRR80, the Nanosystems Initiative Munich (NIM) by the German Excellence Initiative, and the European Research Council (ERC) under the European Union’s Horizon 2020 research and innovation program (grant agreement no. 771537). This research was conducted in part at the KITP, which is supported by NSF Grant No. NSF PHY-1748958. MH acknowledges support from the Deutsche Forschungsgemeinschaft via the Gottfried Wilhelm Leibniz Prize program.

-
- [1] I. Bloch, J. Dalibard, and W. Zwerger, *Rev. Mod. Phys.*, **80**, 885 (2008).
 [2] R. Blatt and C. F. Roos, *Nature Physics*, **8**, 277 (2012).

- [3] I. Bloch, J. Dalibard, and S. Nascimbène, *Nature Physics*, **8**, 267 (2012).
 [4] I. M. Georgescu, S. Ashhab, and F. Nori, *Reviews of Modern Physics*, **86**, 153 (2014), [arXiv:1308.6253 \[quant-ph\]](#).
 [5] M. Schreiber, S. S. Hodgman, P. Bordia, H. P. Lüschen, M. H. Fischer, R. Vosk, E. Altman, U. Schneider, and I. Bloch, *Science*, **349**, 842 (2015), ISSN 0036-8075.
 [6] J.-y. Choi, S. Hild, J. Zeiher, P. Schauß, A. Rubio-Abadal, T. Yefsah, V. Khemani, D. A. Huse, I. Bloch, and C. Gross, *Science*, **352**, 1547 (2016), ISSN 0036-8075.
 [7] J. Smith, A. Lee, P. Richerme, B. Neyenhuis, P. W. Hess, P. Hauke, M. Heyl, D. A. Huse, and C. Monroe, *Nat. Phys.*, **advance online publication** (2016), ISSN 1745-2481, letter.
 [8] P. Bordia, H. P. Lüschen, S. S. Hodgman, M. Schreiber, I. Bloch, and U. Schneider, *Phys. Rev. Lett.*, **116**, 140401 (2016).
 [9] H. P. Lüschen, P. Bordia, S. Scherg, F. Alet, E. Altman, U. Schneider, and I. Bloch, *Phys. Rev. Lett.*, **119**, 260401 (2017).
 [10] D. Basko, I. Aleiner, and B. Altshuler, *Annals of Physics*, **321**, 1126 (2006), ISSN 0003-4916.
 [11] R. Nandkishore and D. A. Huse, *Annual Review of Condensed Matter Physics*, **6**, 15 (2015), <https://doi.org/10.1146/annurev-conmatphys-031214-014726>.
 [12] D. A. Abanin, E. Altman, I. Bloch, and M. Serbyn, *ArXiv e-prints* (2018), [arXiv:1804.11065 \[cond-mat.dis-nn\]](#).
 [13] F. Alet and N. Laflorencie, *Comptes Rendus Physique* (2018), ISSN 1631-0705, doi: <https://doi.org/10.1016/j.crhy.2018.03.003>.
 [14] P. W. Anderson, *Phys. Rev.*, **109**, 1492 (1958).
 [15] J. H. Bardarson, F. Pollmann, and J. E. Moore, *Phys. Rev. Lett.*, **109**, 017202 (2012).
 [16] M. Žnidarič, T. c. v. Prosen, and P. Prelovšek, *Phys. Rev. B*, **77**, 064426 (2008).
 [17] M. Serbyn, Z. Papić, and D. A. Abanin, *Phys. Rev. Lett.*, **110**, 260601 (2013).
 [18] M. Žnidarič, *Phys. Rev. B*, **97**, 214202 (2018).
 [19] E. Canovi, D. Rossini, R. Fazio, G. E. Santoro, and A. Silva, *Phys. Rev. B*, **83**, 094431 (2011).
 [20] M. Serbyn, Z. Papić, and D. A. Abanin, *Phys. Rev. B*, **90**, 174302 (2014).
 [21] R. Singh, J. H. Bardarson, and F. Pollmann, *New Journal of Physics*, **18**, 023046 (2016).
 [22] M. C. Bañuls, N. Y. Yao, S. Choi, M. D. Lukin, and J. I. Cirac, *Phys. Rev. B*, **96**, 174201 (2017).
 [23] S. L. Braunstein and C. M. Caves, *Phys. Rev. Lett.*, **72**, 3439 (1994).
 [24] P. Hauke, M. Heyl, L. Tagliacozzo, and P. Zoller, *Nature Physics*, **12**, 778 EP (2016), article.
 [25] D. Petz and C. Ghinea, *Quantum Probability and Related Topics*, , 261 (2011), [arXiv:1008.2417 \[quant-ph\]](#).
 [26] H. Strobel, W. Muessel, D. Linnemann, T. Zibold, D. B. Hume, L. Pezzè, A. Smerzi, and M. K. Oberthaler, *Science*, **345**, 424 (2014).
 [27] G. Tóth, *Physical Review A*, **85**, 022322 (2012), [arXiv:1006.4368 \[quant-ph\]](#).
 [28] P. Hyllus, W. Laskowski, R. Kischek, C. Schwemmer, W. Wiczkorek, H. Weinfurter, L. Pezzè, and A. Smerzi, *Physical Review A*, **85**, 022321 (2012), [arXiv:1006.4366 \[quant-ph\]](#).

- [29] S. J. Thomson and M. Schiró, Phys. Rev. B, **97**, 060201 (2018).
- [30] A. Lukin, M. Rispoli, R. Schittko, M. E. Tai, A. M. Kaufman, S. Choi, V. Khemani, J. Léonard, and M. Greiner, arXiv e-prints, arXiv:1805.09819 (2018), [arXiv:1805.09819 \[cond-mat.quant-gas\]](#).
- [31] M. Cheneau, P. Barmettler, D. Poletti, M. Endres, P. Schauß, T. Fukuhara, C. Gross, I. Bloch, C. Kollath, and S. Kuhr, *Nature*, **481**, 484 EP (2012).
- [32] G. Carleo, F. Becca, L. Sanchez-Palencia, S. Sorella, and M. Fabrizio, Phys. Rev. A, **89**, 031602 (2014).
- [33] A. M. Luchli and C. Kollath, Journal of Statistical Mechanics: Theory and Experiment, **2008**, P05018 (2008).
- [34] K. Najafi, M. A. Rajabpour, and J. Viti, Phys. Rev. B, **97**, 205103 (2018).
- [35] L. Bonnes, F. H. L. Essler, and A. M. Läuchli, Phys. Rev. Lett., **113**, 187203 (2014).
- [36] L. Barbiero and L. Dell'Anna, Phys. Rev. B, **96**, 064303 (2017).
- [37] J. Z. Imbrie, Journal of Statistical Physics, **163**, 998 (2016), ISSN 1572-9613.
- [38] B. Bauer and C. Nayak, *Journal of Statistical Mechanics: Theory and Experiment*, **2013**, P09005 (2013).
- [39] A. Chandran, I. H. Kim, G. Vidal, and D. A. Abanin, Phys. Rev. B, **91**, 085425 (2015).
- [40] V. Ros, M. Muller, and A. Scardicchio, Nuclear Physics B, **891**, 420 (2015), ISSN 0550-3213.
- [41] D. A. Huse, R. Nandkishore, and V. Oganesyan, Phys. Rev. B, **90**, 174202 (2014).
- [42] M. Serbyn, Z. Papić, and D. A. Abanin, Phys. Rev. Lett., **111**, 127201 (2013).
- [43] N. Pancotti, M. Knap, D. A. Huse, J. I. Cirac, and M. C. Bañuls, Phys. Rev. B, **97**, 094206 (2018).
- [44] L. Rademaker, M. Ortuo, and A. M. Somoza, Annalen der Physik, **529**, 1600322.
- [45] M. H. Fischer, M. Maksymenko, and E. Altman, Phys. Rev. Lett., **116**, 160401 (2016).
- [46] L. Rademaker, M. Ortuno, and A. M. Somoza, ArXiv e-prints (2016), [arXiv:1610.06238 \[cond-mat.str-el\]](#).
- [47] See Supplemental Material for a statistical analysis of the discarded elements $\mathcal{B}_{l,m,n,k}$.
- [48] M. E. Peskin and D. V. Schroeder, *An Introduction to quantum field theory* (Addison-Wesley, Reading, USA, 1995) ISBN 9780201503975, 0201503972.
- [49] F. Iemini, A. Russomanno, D. Rossini, A. Scardicchio, and R. Fazio, Phys. Rev. B, **94**, 214206 (2016).
- [50] R. Vasseur, S. A. Parameswaran, and J. E. Moore, Phys. Rev. B, **91**, 140202 (2015).
- [51] S. Vardhan, G. De Tomasi, M. Heyl, E. J. Heller, and F. Pollmann, Phys. Rev. Lett., **119**, 016802 (2017).
- [52] E. V. H. Doggen, F. Schindler, K. S. Tikhonov, A. D. Mirlin, T. Neupert, D. G. Polyakov, and I. V. Gornyi, ArXiv e-prints (2018), [arXiv:1807.05051 \[cond-mat.dis-nn\]](#).
- [53] M. Žnidarič, T. c. v. Prosen, and P. Prelovšek, Phys. Rev. B, **77**, 064426 (2008).
- [54] S. Bera, G. De Tomasi, F. Weiner, and F. Evers, Phys. Rev. Lett., **118**, 196801 (2017).
- [55] D. J. Luitz, N. Laflorencie, and F. Alet, Phys. Rev. B, **91**, 081103 (2015).
- [56] A. Pal and D. A. Huse, Phys. Rev. B, **82**, 174411 (2010).
- [57] S. Bera, H. Schomerus, F. Heidrich-Meisner, and J. H. Bardarson, Phys. Rev. Lett., **115**, 046603 (2015).
- [58] G. De Tomasi, S. Bera, J. H. Bardarson, and F. Pollmann, Phys. Rev. Lett., **118**, 016804 (2017).
- [59] S. Bera and A. Lakshminarayan, Phys. Rev. B, **93**, 134204 (2016).
- [60] M. Serbyn, Z. Papić, and D. A. Abanin, Phys. Rev. X, **5**, 041047 (2015).
- [61] T. B. Wahl, A. Pal, and S. H. Simon, ArXiv e-prints (2017), [arXiv:1711.02678 \[cond-mat.dis-nn\]](#).
- [62] W. De Roeck and J. Z. Imbrie, Philosophical Transactions of the Royal Society of London Series A, **375**, 20160422 (2017), [arXiv:1705.00756 \[math-ph\]](#).
- [63] I.-D. Potirniche, S. Banerjee, and E. Altman, Phys. Rev. B, **99**, 205149 (2019).
- [64] D. M. Kennes, arXiv e-prints, arXiv:1811.04126 (2018), [arXiv:1811.04126 \[cond-mat.dis-nn\]](#).
- [65] H. Thérieniaut, Z. Lan, and F. Alet, arXiv e-prints, arXiv:1902.04091 (2019), [arXiv:1902.04091 \[cond-mat.dis-nn\]](#).
- [66] For additional comparing data see the Supplemental material.
- [67] See Supplemental Material for a statistical analysis of the discarded off-diagonal elements $\mathcal{B}_{l,m,n,k}$.
- [68] G. De Tomasi, Phys. Rev. B, **99**, 054204 (2019).
- [69] T. Botzung, D. Vodola, P. Naldesi, M. Müller, E. Ercolessi, and G. Pupillo, arXiv e-prints, arXiv:1810.09779 (2018), [arXiv:1810.09779 \[cond-mat.dis-nn\]](#).
- [70] A. Safavi-Naini, M. L. Wall, O. L. Acevedo, A. M. Rey, and R. M. Nandkishore, Phys. Rev. A, **99**, 033610 (2019).
- [71] A. O. Maksymov and A. L. Burin, arXiv e-prints, arXiv:1905.02286 (2019), [arXiv:1905.02286 \[cond-mat.dis-nn\]](#).
- [72] D.-L. Deng, X. Li, J. H. Pixley, Y.-L. Wu, and S. Das Sarma, Phys. Rev. B, **95**, 024202 (2017).
- [73] S. Sahu, S. Xu, and B. Swingle, arXiv e-prints, arXiv:1807.06086 (2018), [arXiv:1807.06086 \[cond-mat.str-el\]](#).
- [74] See Supplemental Material for a further analysis of the two-point correlation function $\mathcal{C}_x(t)$.
- [75] S. Inglis and L. Pollet, Phys. Rev. Lett., **117**, 120402 (2016).
- [76] For additional data see the Supplemental material.
- [77] For additional data see the Supplemental material.
- [78] P. Bordia, H. Lüschen, U. Schneider, M. Knap, and I. Bloch, Nature Physics, **13**, 460 (2017).
- [79] S. Choi, J. Choi, R. Landig, G. Kucsko, H. Zhou, J. Isoya, F. Jelezko, S. Onoda, H. Sumiya, V. Khemani, C. von Keyserlingk, N. Y. Yao, E. Demler, and M. D. Lukin, Nature (London), **543**, 221 (2017).
- [80] J. Zhang, P. W. Hess, A. Kyprianidis, P. Becker, A. Lee, J. Smith, G. Pagano, I. D. Potirniche, A. C. Potter, A. Vishwanath, N. Y. Yao, and C. Monroe, Nature (London), **543**, 217 (2017).
- [81] L.-N. Wu, A. Schnell, G. D. Tomasi, M. Heyl, and A. Eckardt, New Journal of Physics, **21**, 063026 (2019).
- [82] R. Nandkishore, S. Gopalakrishnan, and D. A. Huse, Phys. Rev. B, **90**, 064203 (2014).
- [83] K. Hyatt, J. R. Garrison, A. C. Potter, and B. Bauer, Phys. Rev. B, **95**, 035132 (2017).
- [84] E. Levi, M. Heyl, I. Lesanovsky, and J. P. Garrahan, Phys. Rev. Lett., **116**, 237203 (2016).
- [85] M. Schmitt and M. Heyl, SciPost Phys., **4**, 013 (2018).
- [86] G. Carleo and M. Troyer, Science, **355**, 602 (2017).
- [87] S. A. Weidinger, S. Gopalakrishnan, and M. Knap, Phys. Rev. B, **98**, 224205 (2018).
- [88] I. Peschel and V. Eisler, *Journal of Physics A: Mathe-*

- mathematical and Theoretical, **42**, 504003 (2009).
- [89] B. Kramer and A. MacKinnon, *Reports on Progress in Physics*, **56**, 1469 (1993).

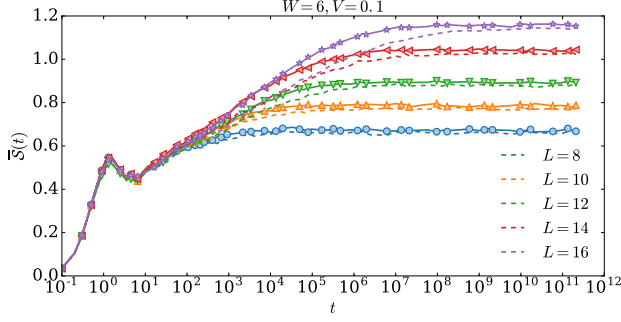


FIG. 5. $\bar{\mathcal{S}}(t)$ evolved with \hat{H} and with \hat{H}^{eff} (dashed-line) for the one-dimensional case for $W = 6$, $V = 0.1$ and several system sizes L .

SUPPLEMENTAL MATERIAL TO SOLVING EFFICIENTLY THE DYNAMICS OF MANY-BODY LOCALIZED SYSTEMS AT STRONG DISORDER

Using Free-Fermion Techniques— The effective model to describe an MBL-phase in the weak-interactions regime reads

$$\hat{H}^{\text{eff}} = \sum_l \epsilon_l \hat{\eta}_l^\dagger \hat{\eta}_l + \sum_{l,m} \mathcal{B}_{l,m} \hat{\eta}_l^\dagger \hat{\eta}_l \hat{\eta}_m^\dagger \hat{\eta}_m, \quad (8)$$

where $\hat{\eta}_l^\dagger = \sum_x \phi_l(\mathbf{i}) \hat{c}_x^\dagger$ with $\{\phi_l\}$ and $\{\epsilon_l\}$ respectively the single-particle wavefunctions and eigenvalues. The coefficient $\{\mathcal{B}_{l,m}\}$ are given by

$$\mathcal{B}_{l,m} = V \sum_{(\mathbf{i},\mathbf{j})} [\phi_l(\mathbf{i}) \phi_m(\mathbf{i}) \phi_l(\mathbf{j}) \phi_m(\mathbf{j}) - |\phi_l(\mathbf{i})|^2 |\phi_m(\mathbf{j})|^2]. \quad (9)$$

In this section, we give an example to show how to calculate efficiently the expectation values of local observables if the quantum evolution is performed using the Hamiltonian \hat{H}^{eff} . Let's consider the density-operator $\hat{n}_x = \hat{c}_x^\dagger \hat{c}_x$

$$\langle \hat{n}_x \rangle = \sum_{l,m} \phi_l(x) \phi_m(x) e^{it(\epsilon_l - \epsilon_m)} \langle \hat{\eta}_l^\dagger e^{it \sum_p (\tilde{\mathcal{B}}_{l,p} - \tilde{\mathcal{B}}_{p,m})} \hat{\eta}_p^\dagger \hat{\eta}_p \hat{\eta}_m \rangle, \quad (10)$$

where $\tilde{\mathcal{B}}_{l,m} = \mathcal{B}_{l,m} + \mathcal{B}_{m,l}$. In Eq. 10 we have used the exact time-dependence of the operators $\{\hat{\eta}_l^\dagger\}$

$$\hat{\eta}_l^\dagger(t) = e^{+it\epsilon_l + it \sum_m \tilde{\mathcal{B}}_{l,m} \hat{\eta}_m^\dagger \hat{\eta}_m} \hat{\eta}_l^\dagger. \quad (11)$$

Now, the expectation value $\langle \hat{\eta}_l^\dagger e^{it \sum_p (\tilde{\mathcal{B}}_{l,p} - \tilde{\mathcal{B}}_{p,m})} \hat{\eta}_p^\dagger \hat{\eta}_p \hat{\eta}_m \rangle$ can be calculate with standard free-fermion technique [88], seeing the operator $e^{it \sum_p (\tilde{\mathcal{B}}_{l,p} - \tilde{\mathcal{B}}_{p,m})} \hat{\eta}_p^\dagger \hat{\eta}_p$ a quantum-evolution operator for the quadratic Hamiltonian defined by

$$\hat{H}^{(l,m)} = \sum_p (\tilde{\mathcal{B}}_{l,p} - \tilde{\mathcal{B}}_{m,p}) \hat{\eta}_p^\dagger \hat{\eta}_p. \quad (12)$$

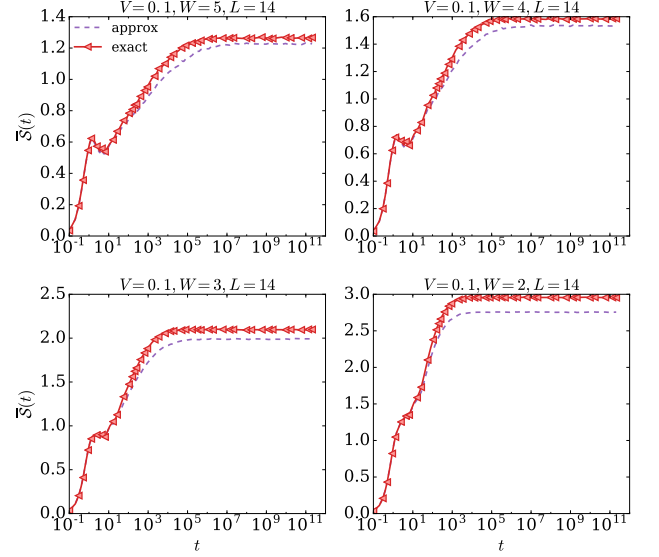


FIG. 6. $\bar{\mathcal{S}}(t)$ evolved with \hat{H} and with \hat{H}^{eff} (dashed-line) for fixed $L = 14$ and $V = 0.1$ and for several disorder strengths W .

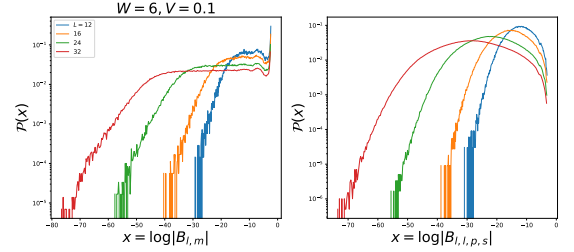


FIG. 7. The left-panel shows the probability distribution $\mathcal{P}(x)$ of $x = \log |\mathcal{B}_{l,m}|$ for several L and $W = 6$ and $V = 0.1$. The right-panel shows $\mathcal{P}(x)$ for $x = \log |\mathcal{B}_{l,l,p,s}|$ for the same values of L , W and V as in the left-panel.

Comparison with exact the exact results— Here, we show further data, comparing the quantum dynamics computed with the exact Hamiltonian \hat{H} and the effective Hamiltonian \hat{H}^{eff} . Figure 5 shows the entanglement entropy $\bar{\mathcal{S}}(t)$ for the one-dimensional system for $V = 0.1$ and $W = 6$, which are the values that have been used in the main text, for several system sizes L . $\mathcal{S}(t)$ independently if calculate with \hat{H} or \hat{H}^{eff} presents the typical log-growth propagation in an MBL-phase ($\sim \xi \log(t)$). Although, the prefactor ξ is different, since our approximation assumes that the localization length in the interacting case (ξ) is the same as the non-interacting one (ξ_{loc}). In other words, for the approximated dynamics we have $\bar{\mathcal{S}}^{\text{approx}}(t) \sim \xi_{\text{loc}} \log t$, while for the exact one $\bar{\mathcal{S}}(t) \sim \xi \log t$ with $\xi \sim \xi_{\text{loc}} + \mathcal{O}(V/W)$, making the relative error $\delta \mathcal{S}(t)$ a bounded function of time. Figure 6 shows $\bar{\mathcal{S}}(t)$ for fixed interaction strength $V = 0.1$ and system size $L = 14$ for several disorder strengths W . As

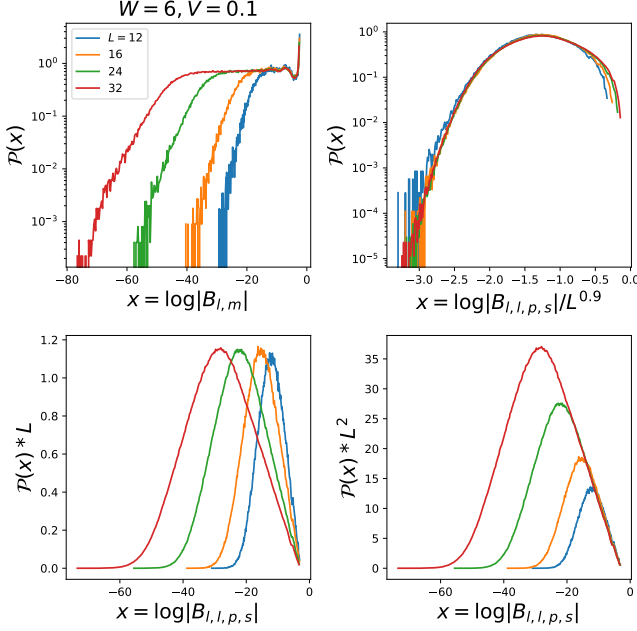


FIG. 8. The figure shows the rescaled probability distribution of $x = \log |\mathcal{B}_{l,m}|$ and $x = \log |\mathcal{B}_{l,l,p,s}|$ with L to underline several characteristics. For $x = \log |\mathcal{B}_{l,m}|$ $\mathcal{P}(x \sim x_{\max}) \leq \mathcal{P}(x \sim 0)$ and in general $\mathcal{P}(x \sim x_{\max}) \sim 1/L$. For $x = \log |\mathcal{B}_{l,l,p,s}|$ $\mathcal{P}(x \sim x_{\max}) \geq \mathcal{P}(x \sim 0)$, in particular $\mathcal{P}(x \sim x_{\max}) \sim 1/L$ and $\mathcal{P}(x \sim 0) \sim 1/L^2$.

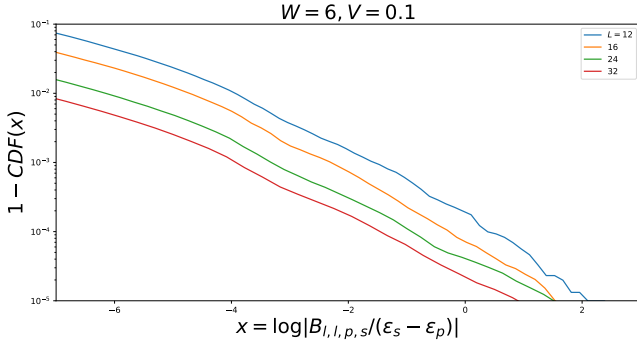


FIG. 9. The figure shows $1 - CDF(x)$ for $x = \log \left| \frac{\mathcal{B}_{l,l,p,s}}{(\epsilon_s - \epsilon_p)} \right|$ for $W = 6$, $V = 0.1$ and several L . The probability of having resonances is $1 - CDF(x \geq 0) \sim 10^{-4}$.

expected our approximation works better for larger disorder strength, in any case independently of W we have $\bar{S}^{\text{approx}}(t) \sim \log t$. A different approach to estimate the error done in our approximation is to calculate the elements of matrix $\mathcal{B}_{l,m,n,p}$ that we have neglected. We will confine our discussion for the 1D case of the Hamiltonian studied in the main text. In this case the interactions elements in the Anderson basis are given by

$$\mathcal{B}_{l,m,n,p} = V \sum_x \phi_l(x) \phi_m(x) \phi_n(x+1) \phi_p(x+1). \quad (13)$$

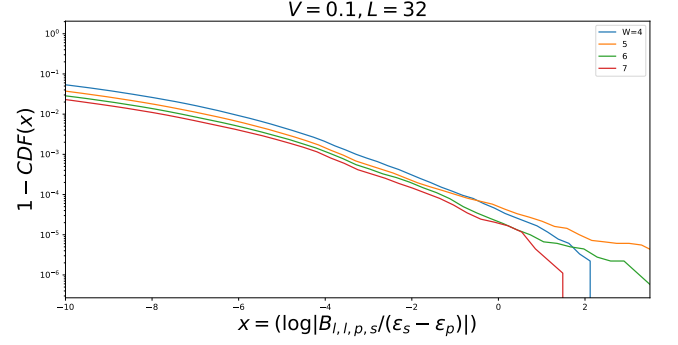


FIG. 10. The figure shows $1 - CDF(x)$ for $x = \log \left| \frac{\mathcal{B}_{l,l,p,s}}{(\epsilon_s - \epsilon_p)} \right|$ for $L = 32$, $V = 0.1$ and several W .

There are two classes of elements that have not been considered

1. Assistant hopping process $\rightarrow \mathcal{B}_{l,l,p,s}$ with $l \neq p \neq s$ (where two energy indexes are the same).
2. $\mathcal{B}_{l,m,n,p}$ with $l \neq m, \neq n \neq p$ (where all indexes are different).

The element of matrix $\mathcal{B}_{l,m,n,p}$ involves the “overlap” between four localized wave functions, thus the second class of the neglected elements is significant smaller compared to the first one. We focus our attention on the assistant hopping terms ($\mathcal{B}_{l,l,p,s}$). Figure 7 shows the probability distribution \mathcal{P} of $\mathcal{B}_{l,m}$ and of $\mathcal{B}_{l,l,p,s}$ over random configurations and energy indexes for $W = 6$ and $V = 0.1$ and several system sizes. It is possible to see that the probability distribution of $\mathcal{B}_{l,m}$ is peaked for value of order one ($\mathcal{B}_{l,m} \sim \mathcal{O}(1)$), while most of them are equally distributed (plateau) to much smaller values,

$$\mathcal{P}(x \sim x_{\max}) \leq \mathcal{P}(x \sim 0) \quad x = \log \mathcal{B}_{l,m}, \quad (14)$$

where x_{\max} is the value of x for which $\mathcal{P}(x)$ has a maximum.

Instead the probability distribution of $\mathcal{B}_{l,l,p,s}$ tend to zero for large values of $\mathcal{B}_{l,l,p,s}$, and most of its elements are distributed to much smaller values. Thus contrarily to the previous case:

$$\mathcal{P}(x \sim x_{\max}) \geq \mathcal{P}(x \sim 0), \quad x = \log \mathcal{B}_{l,l,p,s}. \quad (15)$$

Moreover, in probability the elements $\mathcal{B}_{l,m}$ dominate in magnitude the assistant hopping terms for these values of W and V . It is also important to study the flow of $\mathcal{P}(x)$ with system size. Figure 8 shows the rescaled probability distribution of both $\mathcal{B}_{l,m}$ and $\mathcal{B}_{l,l,p,s}$. $\mathcal{P}(x)$ for $x = \mathcal{B}_{l,m}$ goes to zero as $1/L$. It is due by the fact that in the strong disorder limit most of $\mathcal{B}_{l,m}$'s ($\sim L^2$) will have an exponentially small value since $\mathcal{B}_{l,m}$ involve the “overlap” between two localized wave functions. Nevertheless, some of them will have a large overlap ($\sim L$),

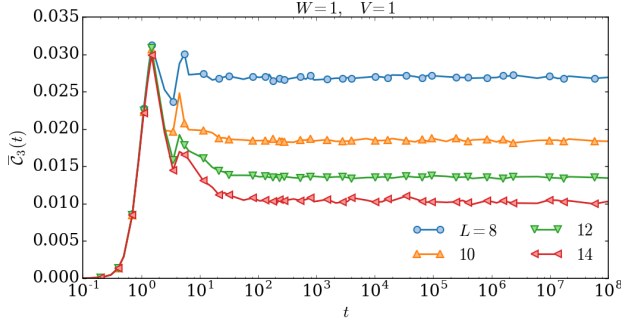


FIG. 11. $C_x(t)$ with fix $x = 3$ and several system sizes L at weak disorder (ergodic phase). After a transient short time dynamic, $C_x(t)$ saturates with time to a L -dependent value which scale exponentially fast to zero with L , $\lim_{t \rightarrow \infty} C_x(t) \sim e^{-\alpha L}$.

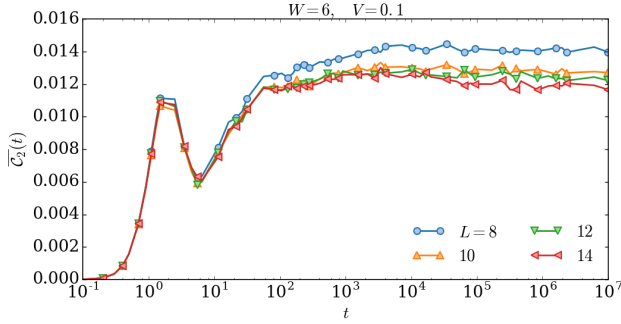


FIG. 12. $C_x(t)$ with fix $x = 2$ and several system sizes L deep in the MBL phase ($W = 6, V = 0.1$). This results are obtained using exact diagonalization. Due to the limitation of system size the expected bending at large time for $C_x(t)$ is only slightly visible.

these terms represent wave functions that are close by localized. As we already discussed most of $\mathcal{B}_{l,l,p,s}$'s (pick of \mathcal{P} shifts to an exponentially small number in L as shown in Fig. 8 ($\mathcal{B}_{l,l,p,s}^{\text{typical}} \sim e^{-\alpha L^\delta}$ with $\delta \approx 0.9$). Moreover the amplitude of having a typical value goes also to zero with L ($\mathcal{P}(x \sim x_{\text{max}}) \sim 1/L$), while the probability of having large value of $\mathcal{B}_{l,l,p,s}$ goes to zero faster ($\mathcal{P}(x = \log |\mathcal{B}_{l,l,p,s}| \sim 0) \sim 1/L^2$).

We also looked for resonances, meaning of the break down of first order perturbation theory and thus the need to go beyond first order in V or to use degenerate perturbation theory. We studied these elements statistically calculating its probability distribution. The probability of having resonances give us an estimation of error done in taking for eigenstates the ones of the non-interacting case. Up to first order in the interaction strength V , the assistant hopping processes ($\mathcal{B}_{l,l,p,s}$) will give a contribution of the form

$$\text{first order in } V \sim \frac{B_{l,l,p,s}}{(\epsilon_s - \epsilon_p)}, \quad (16)$$

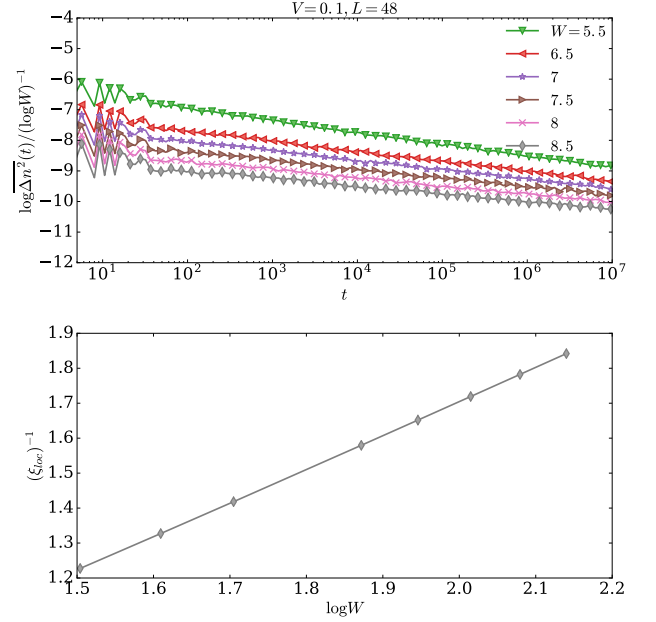


FIG. 13. The top-panel shows the time fluctuation $\overline{\Delta n^2}(t)$ calculated using \hat{H}^{eff} for several W 's in the strong disorder limit and fixed V and L . The initial state is given by $|\psi\rangle = \prod_{s=-L/4}^{L/4} c_{2s}^\dagger |0\rangle$ (charge-density state). The bottom-panel shows ξ_{loc} calculated with transfer-matrix technique at the band-center of the single-particle problem, giving evidence that $\xi_{\text{loc}} \sim \log W^{-1}$.

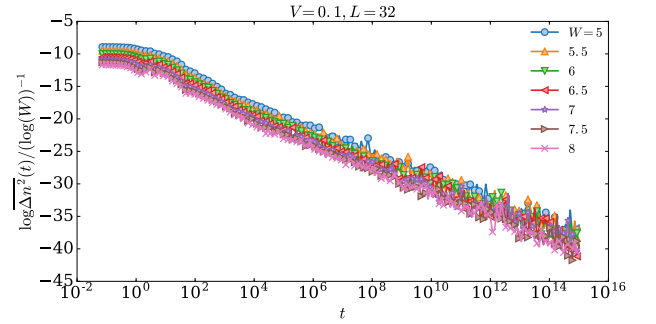


FIG. 14. $\overline{\Delta n^2}(t)$ calculated using \hat{H}^{eff} for several W 's in the strong disorder limit and fixed V and L with initial state $|\psi\rangle = \prod_l^L \frac{\hat{q}_l + \hat{q}_l^\dagger}{\sqrt{2}} |0\rangle$.

where ϵ_l 's are the single-particles eigenenergies. We will say that two energies ϵ_p and ϵ_s are in resonance at first order in V if

$$\left| \frac{B_{l,l,p,s}}{(\epsilon_s - \epsilon_p)} \right| \geq 1. \quad (17)$$

We calculate the cumulative distribution function (CDF)

of the distribution function $\mathcal{P}(x)$ of $x = \log \left| \frac{B_{t,L,p,s}}{(\epsilon_s - \epsilon_p)} \right|$

$$CDF(x) = \int_{-\infty}^x dx \mathcal{P}(x). \quad (18)$$

Figure 9 shows $1 - CDF(x) = \int_x^\infty dx \mathcal{P}(x)$ for the values of W and V used in the main text. The probability of having resonances ($1 - CDF(x \geq 0)$) is of the order of 10^{-4} (less than 1%). This value tells us what is the probability that our approach is inadequate and higher order processes in V should be considered. We repeated this analysis for several value of W (Fig. 10).

The two-point connected correlation function $\mathcal{C}_x(t)$ — In this section we provide a more detailed analysis for the dynamics of the two-point correlation function $\mathcal{C}_x(t)$. In particular, we will use this section also to emphasize the necessity to simulate larger system sizes than the ones accessible by exact diagonalization (ED) in order to understand the right behavior of $\mathcal{C}_x(t)$ in the localized phase.

First, we would like to demonstrate that in a thermal phase $\mathcal{C}_x(t)$ decays to zero with time. Figure 11 shows $\mathcal{C}_x(t)$ for a fix distance $x = 3$ in the ergodic phase ($W = 1$) of the one-dimensional model studied in main text [55]. By definition, at $t = 0$, $\mathcal{C}_x(t) = 0$ and after a transient L -independent propagation, $\mathcal{C}_x(t)$ saturates on long times to a L -dependent value, which shows a marked trend towards zero with L . Moreover, it is possible to show that $\lim_{L \rightarrow \infty} \mathcal{C}_x(t) \sim e^{-\alpha L}$.

That this eventually yields a vanishing correlation function can be understood simply by the fact that the system is fully ergodic. Indeed, at infinite temperature, as we considered in the main text, the long-time steady state can be described by a random state (e.g. the entanglement entropy after a quantum quench saturates to the Page value $\mathcal{S} \sim L/2 \log 2$), so that we can take a quantum average over a random state which yields

$$\lim_{t \rightarrow \infty} \mathcal{C}_x(t) \sim e^{-\alpha L} \quad \alpha > 0, \quad (19)$$

Consequently, such correlators vanish in an ergodic system at least at infinite temperature.

Instead, Fig. 12 shows $\mathcal{C}_x(t)$ for $x = 2$ deep in the MBL phase. In this case the results are obtained using ED to show the importance to be able to simulate larger systems sizes.

Indeed, at large times one can observe a slight bending down of the long-time value of $\mathcal{C}_x(t)$ for increasing L . Nevertheless it is not possible to predict the behavior in the thermodynamic limit due to the limitations in the accessible system sizes with ED. The efficiency of our method allows us now to address much larger system sizes ($L \sim 50$) at arbitrarily large time scales, and thus to give a prediction on the behavior in the thermodynamic limit.

Time fluctuations— In this section, we show further data concerning the time fluctuation of local observables (i.e. \hat{n}_x), which is defined by

$$\Delta n^2(t) = \frac{1}{L} \sum_x \Delta n_x^2(t), \quad (20)$$

where

$$\Delta n_x^2(t) = (\langle \hat{n}_x \rangle(t) - \langle \hat{n}_x \rangle_{\text{time ave.}})^2, \quad (21)$$

and

$$\langle \hat{n}_x \rangle_{\text{time ave.}} = \lim_{T \rightarrow \infty} \frac{1}{T} \int_0^T ds \langle \hat{n}_x \rangle(s), \quad (22)$$

is the long-time average of $\langle \hat{n}_x \rangle(t)$. In the main text we show that the time fluctuation decay algebraically $\Delta n^2(t) \sim t^{-\alpha}$. Moreover, we claim that $\alpha \propto \xi_{\text{loc}}$ [20]. Figure 13 shows $\overline{\Delta n^2}(t)$ for several W 's in the strong disorder limit. For all inspected disorder strengths $\Delta n^2(t)$ decays algebraically for several order of magnitude, the curves have been rescaled to underline that $\alpha \propto \log W^{-1}$. Indeed in the strong disorder limit $\xi_{\text{loc}} \sim \log W^{-1}$, as shown in Fig. 13, where ξ_{loc} has been calculated using standard transfer-matrix technique [89]. Furthermore, in the main text we support the result $\Delta n^2(t) \sim t^{-c\xi_{\text{loc}}}$ with an analytical argument starting from a different initial state $|\psi\rangle = \prod_l^L \frac{\hat{\eta}_l + \hat{\eta}_l^\dagger}{\sqrt{2}} |0\rangle$. Figure 14 shows $\overline{\Delta n^2}(t)$ starting from $|\psi\rangle$ for several disorder strengths W , giving evidence that $\Delta n^2(t) \sim t^{-c\xi_{\text{loc}}}$, with $\xi_{\text{loc}} \sim \log W^{-1}$.